Quantum and Classical Chirps in an Anharmonic Oscillator

Yoni Shalibo, Ya'ara Rofe, Ido Barth, Lazar Friedland,
Radoslaw Bialczack, John M. Martinis and Nadav Katz

Supplementary Information

Materials and methods. The Josephson phase circuit [1] used in the experiment has the following design parameters: critical current $I_0 \approx 1.5\,\mu$A, capacitance C≈1.3 pF and inductance L≈940 pH. The qubit has a tunable frequency f_{01} in the 6-9 GHz range [2]. During the experiment the device is thermally coupled to the mixing chamber of a dilution refrigerator at 30 mK, where thermal excitations of the qubit are negligible.

We use a custom built arbitrary waveform generator (AWG) having a fast (1 ns time resolution), 14-bit digital-to-analog converter to produce both the chirp signal and the measurement pulse. To produce the chirp, we modulate a high-frequency oscillator, having a frequency f_{LO}, using an IQ-mixer. The modulation signals, produced by the AWG, are fed into the I and Q ports of the IQ-mixer to give $\sqrt{I(t)^2+Q(t)^2}\cos\left(2\pi f_{\mathrm{LO}}t+\phi\right)$ at its output, where $\phi=\arctan\left(Q(t)/I(t)\right)$. To produce a frequency shift from the high-frequency oscillator, we keep the amplitude at the output constant while varying the phase ϕ linearly in time; to produce a chirp, we use an accelerating phase: $\phi=2\pi f_0 t-\alpha t^2/2$, where $f_0=f_{\mathrm{in}}-f_{\mathrm{LO}}$, f_{in} is the initial frequency of the chirp, and α is the chirp rate.

To properly measure the locking probability P_{locked}, it is generally desirable to have the maximal possible chirp bandwidth $\Delta f=f_{\mathrm{in}}-f_{\mathrm{fin}}$ (f_{fin} being the final frequency of the chirp) in order to raise the energy expectation of the locked population higher. This leads to a better distinguishability between the locked and the unlocked population at the end of the chirp and correspondingly to an increased measurement fidelity of the locking probability, as illustrated in Fig S1. The AWG's bandwidth limitation results in an error of up to ∼10 % in P_{locked} at large anharmonicity (Fig. 1a), however it does not affect the threshold position in Fig. 4a. We use the maximal bandwidth (600 MHz), varying the modulation frequency from 300 MHz to -300 MHz [3], and setting the oscillator frequency f_{LO} 200 MHz lower than the qubit frequency f_{01}. The additional 100 MHz of bandwidth beyond the qubit frequency

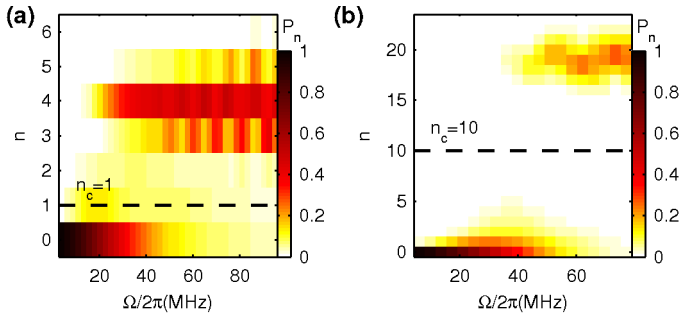

Figure S1: Level occupation of a bifurcated state after chirp in simulation, as a function of amplitude. Chirp parameters: (a) $\beta_r = 0.023$, $\alpha/2\pi = 6\,\mathrm{MHz/ns}$ and (b) $\beta_r = 0.002$, $\alpha/2\pi = 12\,\mathrm{MHz/ns}$. $\Delta f = 600\,\mathrm{MHz}$ and $f_{01} - f_{\mathrm{fin}} = 500\,\mathrm{MHz}$ in both. The locked and unlocked populations are discriminated by a level cutoff n_c (dashed lines), which is experimentally realized by a calibrated measurement pulse (see dashed line in Fig. 3e). At large anharmonicity relative to the chirp bandwidth (a), the locked and unlocked populations partially overlap, leading to a maximal error of $\sim$10 % in P_{locked} for the parameters used in the experiments.

is taken to reduce the sensitivity of the threshold to initial condition [4].

Data processing. To extract the state occupation probabilities P_{n}, we use the escape probabilities vs. measurement amplitude data ("escape curve", $P_{\mathrm{esc}}(I_{\mathrm{meas}})$). We first measure the single-level escape curves by preparing the system in an $|n\rangle$ state, and then measuring the escape probability as a function of I_{meas} (see Fig. S2a). Once the single-level escape curves $P^{\mathrm{n}}_{\mathrm{esc}}(I_{\mathrm{meas}})$ are at hand, we decompose the measured escape curve of an arbitrary state into the single-level basis $P^{\mathrm{n}}_{\mathrm{esc}}(I_{\mathrm{meas}})$ by optimizing the solution P_{n} to the set of J equations $P_{\mathrm{esc}}(I^j_{\mathrm{meas}}) = \sum_n P_{\mathrm{n}} P^{\mathrm{n}}_{\mathrm{esc}}(I^j_{\mathrm{meas}})$, where $j = 1, .., J$. Generating the $|n\rangle$ state becomes increasingly difficult at a larger n, due to the short lifetime of excited states. The procedure is even more problematic when the anharmonicity β is small and longer pulses are required to create the target state with reasonable fidelity. In practice, at the small anharmonicity regime that is used in the state dynamics measurement (see main paper), where $\beta/2\pi = 18\,\mathrm{MHz}$, it becomes impossible to prepare the system in an $|n\rangle$ state, even for $n > 1$. Instead, we use the first excited state escape curve, shifted by $\delta I_{\mathrm{meas}}(n) = I_{\mathrm{meas}}(0) - I_{\mathrm{meas}}(n)$ as an approximate escape curve. This approximation is supported by WKB calculation (see below). To determine the position of the escape curves we use the chirp data itself: for a given state, the measured escape curve contains information about the position of the single

level escape curves. As seen in Fig. S2a, the position of these escape curves (defined as the point where the single-level escape curve increases to 0.5 of its maximal value) is determined from the positions of the peaks in the derivative $\partial P_{\rm esc}(I_{\rm meas})/\partial t$. Due to the finite width of the single level escape curves, the peak corresponding to a certain level is visible only when the level occupation is sufficiently large. To find $I_{\rm meas}(n)$ for all the relevant levels, we sum the derivative over all the times along the chirp, as illustrated in Fig. S2b. The extracted $I_{\rm meas}(n)$ values are plotted in Fig. S2c (red circles).

Simulation. To check the validity of our estimate for the escape curves, we calculate them numerically using the WKB approximation of the level dependent tunneling rates [5]:

$$\Gamma_{\rm n} = f_{\rm n} exp(-2iS_{\rm n}/\hbar), \tag{1}$$

where $S_{\rm n} = \int_{\delta_2}^{\delta_3} |p_{\rm n}(\delta)|\, d\delta$ is the action, $\delta_{\rm i}$ are the classical turning points defined in Fig. S2d, $p_{\rm n}(\delta) = \sqrt{2m\left(E_{\rm n} - U(\delta)\right)}$ is the momentum, $E_{\rm n}$ is the energy of the n^{th} level, $U(\delta)$ is the potential energy, $f_{\rm n}$ is the classical attempt frequency, $m = C\left(\Phi_0/2\pi\right)^2$ is the effective mass and $\Phi_0 = h/2e$ is a flux quantum. f_n is calculated using the classical oscillation time: $f_{\rm n} = 1/\tau$, where $\tau = \oint dt = 2\int_{\delta_1}^{\delta_2} \frac{d\delta}{p(\delta)/m}$. The energies of the system are calculated by diagonalizing the system Hamiltonian:

$$\hat{H} = -\frac{2e^2}{C}\frac{d^2}{d\hat{\delta}^2} - \frac{I_0\Phi_0}{2\pi}\cos\hat{\delta} + \frac{1}{2L}\left(\Phi_{\rm ext} - \frac{\hat{\delta}\Phi_0}{2\pi}\right)^2. \tag{2}$$

The circuit parameters are found by best-fitting the calculated lowest frequencies f_{01} and f_{12} to the measured ones and fixing the number of levels in the well to 50 (the number of levels in the well is obtained from extrapolating the experimental points in Fig. S2c to $I_{\rm meas}(P_{\rm esc} = 0.5) = 0$) [6]. The single-level escape curves are then given by, $P^{\rm n}_{\rm esc}(I_{\rm meas}) = 1 - \exp(-\Gamma_{\rm n}(I_{\rm meas})\Delta t)$, where Δt is the measurement pulse length. The calculated positions of the single-level escape curves are plotted in Fig. S2c (solid blue line).

We simulate the state dynamics of our N-level system under a frequency-chirped drive by propagating its density matrix ρ with the time evolution operator $U = \exp(iH_{\rm N}\Delta t)$. The N-level Hamiltonian is calculated in the rotating frame of the drive, with the rotating wave approximation [7] applied:

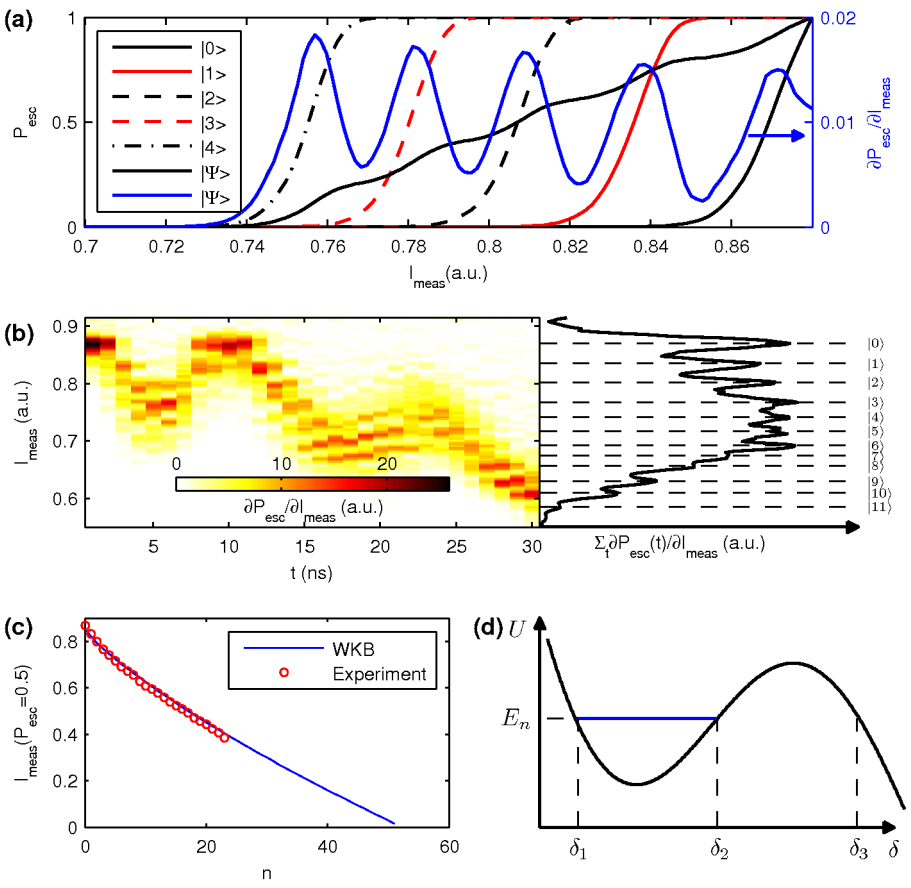

Figure S2: (a) Left axis: Calculated escape curves of single level states, and of the state $|\Psi\rangle = 1/\sqrt{5}\,(|0\rangle + |1\rangle + |2\rangle + |3\rangle + |4\rangle)$. Right axis: derivative of the escape curve of $|\Psi\rangle$. (b) Left panel: Derivative of the escape curve as a function measurement amplitude and time along the chirp shown in Fig. 2c. Right panel: Temporal sum of the data shown in the left panel, as a function of measurement amplitude. (c) Experimental and calculated positions of the escape curve. The WKB curve is calculated from the level dependent tunneling rates, based on the calculated energies using the best fitted circuit parameters. (d) Potential energy of the circuit used for WKB calculation, with classical turning points.

$$H_{\mathrm{N}} = \hbar \begin{pmatrix} 0 & \Omega/2 & 0 & 0 & \dots & 0 \\ \Omega/2 & -\Delta & \sqrt{2}\Omega/2 & 0 & & 0 \\ 0 & \sqrt{2}\Omega/2 & \epsilon_{02} - 2\Delta & \sqrt{3}\Omega/2 & & 0 \\ 0 & 0 & \sqrt{3}\Omega/2 & \epsilon_{03} - 3\Delta & & \vdots \\ \vdots & & & & \ddots & \sqrt{N}\Omega \\ 0 & 0 & 0 & \dots & \sqrt{N}\Omega & \epsilon_{0,\mathrm{N}} - (N-1)\Delta \end{pmatrix}, \tag{3}$$

where$\epsilon_{0,\mathrm{n}} = 2\pi\left(f_{0,\mathrm{n}} - n f_{0,1}\right)$ is the cumulative anharmonicity at the n^{th} level and $\Delta = \Delta(t) = 2\pi\left(f(t) - f_{01}\right)$ is the frequency detuning of the drive and $h = 2\pi\hbar$ is Planck's constant. The Rabi amplitude Ω is taken as a real constant during the chirp, and the detuning is a linearly decreasing function starting at $+2\pi\cdot$100 MHz and ending at -$2\pi\cdot$500 MHz, as done in the experiment. The cumulative anharmonicities $\epsilon_{0,\mathrm{n}}$ are calculated from the diagonalization of the system Hamiltonian (Eq. 2). The simulation neglects deviations of matrix elements due to the drive, beyond the harmonic oscillator approximation. Namely, for $m \neq n \pm 1$, we set $\left\langle n \left| \hat{\delta} \right| m \right\rangle = 0$, and for $m = n \pm 1$ we set $\left\langle n \left| \hat{\delta} \right| m \right\rangle = \sqrt{n+1}, \sqrt{n}$. We find for the first order matrix elements ($m = n \pm 1$) a maximal deviation of order $\sim 10^{-2}$ at the largest anharmonicity, and highest states. The second order matrix elements ($m = n \pm 2$) have a maximal value of order $\sim 10^{-1}$, relative to the first order term at the same m value. Higher order elements are smaller than $\sim 10^{-4}$. For $m = n$, the contribution to the energies for the range of drive amplitudes used in the experiment is small compared with the rotating frame energies. A separate simulation taking into account all the matrix elements, without the rotating wave approximation, yields identical results in the simulations shown below (see Fig. S3b,d) to within a $\sim 10^{-2}$ deviation. Decoherence is taken into account using quantum operations [8] for amplitude and phase damping.

In Fig. S3 we plot the level populations as a function of time during the chirp shown in Fig. 2, compared with the experimental data. The simulation is calculated with no fit parameters and includes the effect of energy and phase damping. The energies at large anharmonicity (Fig. S3b) are estimated from spectroscopy data, while for small anharmonicity (Fig. S3d) they are extracted from the diagonalization of the system Hamiltonian. The experimental data and simulation agree qualitatively in both regimes. At large anharmonicity, the lengths of the "steps" are slightly different in the simulation due to the error in determining the bare transition frequencies (obtained from high power spectroscopy, where shifts and broadenings

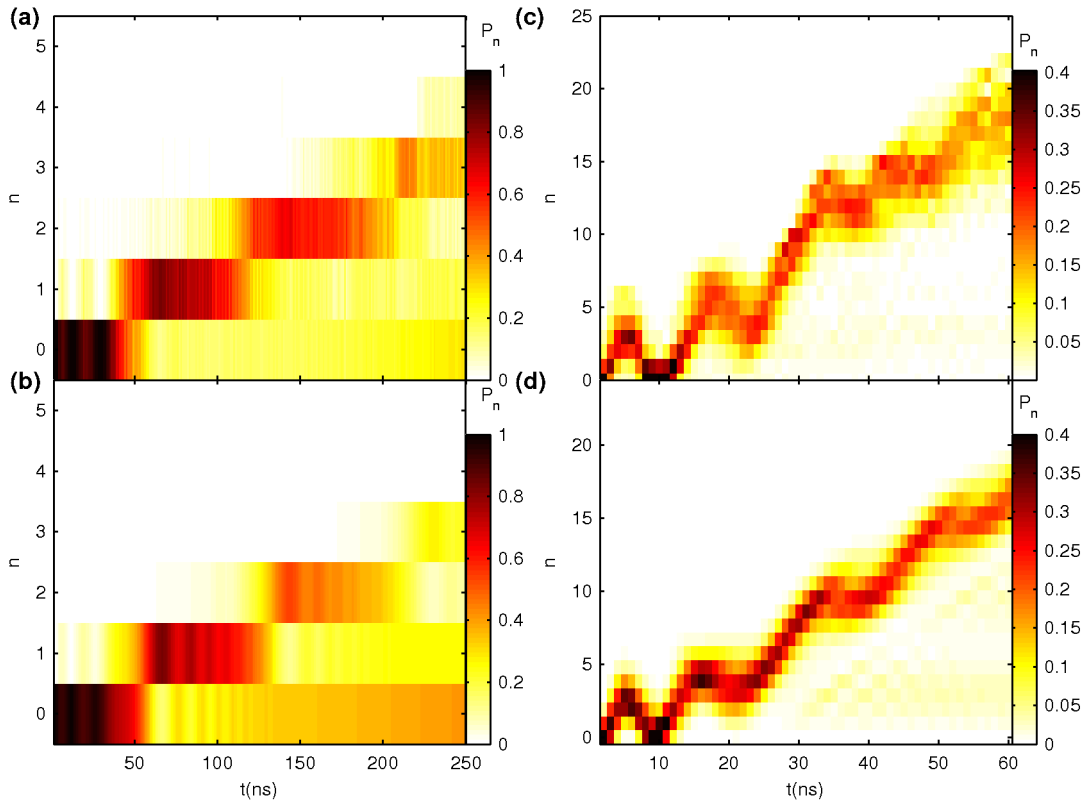

Figure S3: (a) Experimental data and (b) simulation of the dynamics experiment at large anharmonicity ($\beta/2\pi$=158 MHz) shown in Fig. 2b. (c) Experimental data and (d) simulation of the dynamics experiment at small anharmonicity ($\beta/2\pi$=18 MHz) shown in Fig. 2b.

are significant). At small anharmonicity, we see a smearing of the oscillations at higher states. This is mainly due to the frequency dependent drive amplitude. In both measurements (and simulations), we used a frequency dependent drive which decreases along the chirp as $\sqrt{n(t)}$ (where $n(t)$ is the expected average state number as a function of time) to compensate for the increasing drive coupling at higher states which increases the mixing between the levels. This, however, does not affect the locking condition which is determined from the drive amplitude at the first transition.

We compute the locking probability in the simulation by defining a cutoff n_c at intermediate levels: $P_{\text{locked}} = \sum_{n>n_c} \rho_{\text{nn}}$, where the level population vanishes (see Fig. S1). The results of this simulation are shown in Fig. 4b. All the parameters in the simulation (anharmonicities, chirp rates, drive amplitudes, and decay times) are those used/measured in the experiment.

We find that the simulation reproduces the main features of the experiment: the position of the threshold as a function of $\beta/\sqrt{\alpha}$ and consequently the transition between autoresonance and ladder climbing. The simuation (as well as the experiment), displays slow averaged features with superimposed fast oscillations. These features represent interference between adjacent levels in the driven system. We observe that the fast oscillations strongly depend on initial conditions (the distance from resonance), while the averaged slow oscillations are characteristic to the transition between the quantum and classical dynamics.

The coherence time T_2 only weakly affects the threshold in our experiment. This claim is supported by the fact that the measured threshold follows that of the decoherence free simulation despite the chirp time being longer than T_2. In this simulation , we see that at small anharmonicity, far off-diagonal elements of the density matrix (high-order coherence terms) of a high-amplitude phase-locked wavepacket are negligible and the phase space (Wigner) representation of the wavepacket is similar to the one calculated for a classical system [9, 10]. At large anharmonicity, we find that only the first order coherences of the state ($\rho_{i,i+1}$ terms of the density matrix) are non-zero and they are significantly populated for short times (compared to the relevant dephasing time), during transitions between neighboring levels.

Theory of held drive. The locking time $T_{\text{locked}} = W^{-1}$ (where W is the decay rate from the locked state of the nonlinear resonance) is calculated by Dykman et al. in the framework of quantum activation [11]. It is shown that in the case of weak damping and at low temperatures ($k_{\text{B}}T \ll hf_{01}$), the locking time is given by:

$$T_{\text{locked}} = c\exp(\eta\Omega/2\pi), \tag{4}$$

where, $\eta \approx 4/\sqrt{f_{01}\left|f_{\text{fin}} - f_{01}\right|\beta_r}$, and c is a constant on the order of T_1. This result is valid for intermediate drive amplitudes:

$$\frac{1}{2\pi T_1}\sqrt{\frac{4\left|f_{\text{fin}} - f_{01}\right|}{\beta_r f_{01}}} \ll \Omega/2\pi \ll \left|f_{\text{fin}} - f_{01}\right|\sqrt{\frac{4\left|f_{\text{fin}} - f_{01}\right|}{\beta_r f_{01}}}, \tag{5}$$

as is the case in our experiment, where these conditions translate to $4\,\text{MHz} \ll \Omega/2\pi \ll 3.7\,\text{GHz}$.

In this theory, the dynamics are considered to be classical while the noise is quantum, and is associated with zero-point fluctuations. Moreover, the expression for the locking time coincides with the classical formula for the escape time [12], when the classical temperature

in [12] is replaced by an effective temperature, $T_{\text{eff}} = (hf_{01}/2k_{\text{B}})\coth(hf_{01}/2k_{\text{B}}T)$. A more intuitive, but equivalent theory for the locking time is given by Dykman et al. [13] where the escape time from an effective potential well associated with the phase-locked state is calculated. The potential barrier in this case scales as the drive amplitude.

We find good agreement between the simulation of this experiment at several anharmonicities and the scaling predicted by Eq. 4. The theoretical prediction of the factor η, calculated using the experimental parameters (see black dashed line in Fig. 3d) is within 15 % from that obtained in the simulation with the same parameters.

---

[1] J. M. Martinis, S. Nam, J. Aumentado, C. Urbina, Phys. Rev. Lett., **89**, 117901 (2002).

[2] The data in Fig. 3d is obtained from a different sample, having similar design parameters and qubit frequency range.

[3] We use a smaller bandwidth only in some of the measurements shown in the parameter space diagram (Fig. 4a) in order to achieve larger $\beta/\sqrt{\alpha}$ values while keeping the chirps shorter than the decay time.

[4] L. Friedland, J. Phys. A: Math. Theor., **41**, 415101 (2008).

[5] J. Ankerhold, Quantum Tunneling in Complex Systems: The Semiclassical Approach (Springer Tracts in Modern Physics) (Springer, 2007).

[6] The Hamiltonian in Eq. 2 is only an approximation of our system. In practice, the inductance may be flux dependent due to the small coupling between the circuit and the SQUID. For this reason, we find it difficult to obtain a good fit of the measured flux dependent energies to the calculated ones. We find that the parameters obtained from the fit have ∼10 % of uncertainty in the flux range used in the calculation.

[7] D. F. Walls, G. J. Milburn, Quantum Optics, 2nd ed. (Springer, 2008).

[8] M. A. Nielsen, I. L. Chuang, Quantum Computation and Quantum Information (Cambridge University Press, 2004).

[9] K. W. Murch *et al.*, Nat. Phys., **7**, 105 (2011).

[10] I. Barth, L. Friedland, O. Gat, A. G. Shagalov, Phys. Rev. A, 84, 013837 (2011).

[11] M. I. Dykman, V. N. Smelyanskiy, Sov. Phys. JETP, **67**, 1769 (1988).

[12] M. I. Dykman, M. A. Krivoglaz, Sov. J. Exp. Theor. Phys., **50**, 30 (1979).

[13] M. I. Dykman, I. B. Schwartz, M. Shapiro, Phys. Rev. E, **72**, 021102 (2005).